Title
The Effect of Contact Area on the Permeability of Fractures

Journal
Journal of Hydrology, 139

Authors
Zimmerman, R.W.
Chen, D.-W.
Cook, N.G.W.

Publication Date
1993-03-01

LBL-32356
UC-400, 810
Preprint

Lawrence Berkeley Laboratory
UNIVERSITY OF CALIFORNIA

EARTH SCIENCES DIVISION

Submitted to Journal of Hydrology

The Effect of Contact Area on the Permeability of Fractures

R.W. Zimmerman, D.-W. Chen, and N.G.W. Cook

March 1992

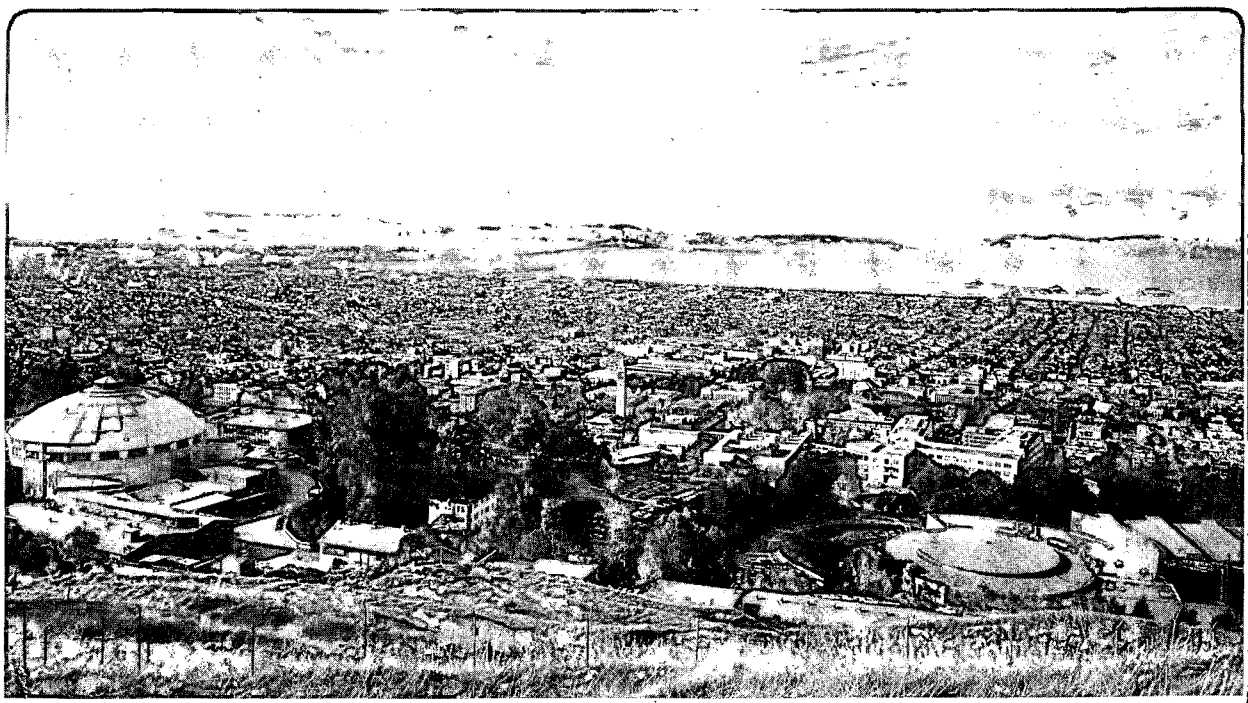

Prepared for the U.S. Department of Energy under Contract Number DE-AC03-76SF00098

DISCLAIMER

LBL-32356

The Effect of Contact Area on the Permeability of Fractures

Robert W. Zimmerman, Di-Wen Chen, and Neville G. W. Cook

Earth Sciences Division
Lawrence Berkeley Laboratory
University of California
Berkeley, California 94720

March 1992

This work was supported by the Director, Office of Civilian Radioactive Waste Management, Repository Technology and Transportation Division, and by the Director, Office of Energy Research, Office of Basic Energy Sciences, under U.S. Department of Energy Contract No. DE-AC03-76SF00098.

The Effect of Contact Area on the Permeability of Fractures

*Robert W. Zimmerman, Di-Wen Chen, and Neville G. W. Cook**

Earth Sciences Division
Lawrence Berkeley Laboratory
University of California
Berkeley, CA 94720

*also: Department of Materials Science and Mineral Engineering
University of California
Berkeley, CA 94720

ABSTRACT

The permeability of a rock fracture is controlled primarily by the geometry of its void space. One effect of void space geometry is to cause the fluid to follow a tortuous path in order to flow around the asperities, which are regions where the two faces of the fracture are in contact. In order to examine the tortuosity induced by the contact area, we consider an idealized fracture consisting of two parallel plates propped open by isolated asperities. Boundary-element calculations, analogue electrical conductivity measurements, and an effective medium approximation are used to study the permeability of fractures with circular, elliptical, and irregular asperity shapes. The permeability is seen to depend not only on the amount of contact area, but also on the shape of the asperities. For circular or elliptical asperities, very accurate estimates are found by using the effective medium theory proposed by Maxwell.

INTRODUCTION

In many geological formations with low matrix permeability, fluid flow takes place predominantly through fractures. Fracture-dominated flow has become increasingly important in various problems of geotechnical interest, particularly those involving underground waste isolation. In some cases flow takes place through a particular fracture or fault, while in other cases the flow is through a network of fractures. In either case, an understanding of the permeability of single fractures is required.

The permeability of a naturally occurring rock fracture depends principally on the geometry of the void space. A typical fracture contains isolated asperity regions where the two rock surfaces are in contact, surrounded by open regions where the two surfaces are separated by an aperture h that may vary from point to point. When fluid flows through such a fracture, it not only must flow around the contact areas, but also has a tendency to preferentially flow through the channels with the largest apertures, since hydraulic conductance is proportional to h^3. In order to successfully model this process, both effects must be taken into account. In this paper, however, attention will be focused on the tortuosity induced by the contact regions. (The effect of roughness in the fracture walls, i.e., variations in the aperture, has been studied by Brown (1987), Pyrak-Nolte et al. (1988), and Zimmerman et al. (1991), among others). Here we consider idealized fractures consisting of two parallel surfaces, with isolated regions of contact. These contact areas have the effect of decreasing the permeability below the value that would pertain to unobstructed flow between parallel plates. Numerical and analytical methods are used to relate this decrease in permeability to the amount of contact area, and to the geometrical structure of the contact areas.

FORMULATION OF PROBLEM

The flow of a Newtonian fluid (such as water) through a fracture is governed by the nonlinear Navier-Stokes equations. Exact solutions to these equations for specific

geometries are usually very difficult to obtain. The exact solution for flow between two parallel plates under a uniform pressure gradient, however, is known (see Schlichting, 1968, p. 77). The velocity profile (across the fracture) for this flow is parabolic, with zero velocity at the upper and lower surfaces to satisfy the no-slip boundary condition. The total fluid flux $\vec{Q}$ (per unit depth in the fracture plane in the direction normal to ∇P) is found by integrating the velocity across the thickness of the channel. This leads to the familiar cubic law $\vec{Q} = -h^3 \nabla P / 12\mu$, where ∇P is the pressure gradient, and μ is the viscosity of the fluid. In terms of Darcy's law, which states that $\vec{Q} = -kh \nabla P / \mu$, the parallel plate geometry has a permeability $k = h^2/12$. In SI units, for instance, ∇P has units of [Pa/m], h has units of [m], and μ has units of [Pa·s]; the flux vector $\vec{Q}$ will therefore have units of [m^2/s]. The *total* volumetric flux can be found by multiplying this value by the fracture depth normal to ∇P.

For a fracture that is modeled as two parallel plates propped open by discrete areas of contact (Fig. 1), the flow cannot be everywhere parallel to the overall pressure gradient, since the fluid must follow a tortuous path as it circumvents the obstacles. If the flow rates are suitably low, and if the aperture h is small relative to the characteristic dimension a of the contact areas (Fig. 1), the flow can be well approximated by "Hele-Shaw" flow (Schlichting, 1968, p. 114). The precise constraint on the velocity is that $Re^* = \rho U h^2 / \mu a << 1$, where Re^* is the reduced Reynolds number, and U is the mean velocity magnitude. In Hele-Shaw flow, the fluid still has a parabolic velocity profile, and the velocity vector $\vec{u}$ at each point is still parallel to the local pressure gradient, but the local pressure gradient is not necessarily equal to the overall macroscopic pressure gradient. The velocity profile for this type of flow is given by

$$\vec{u} = \frac{-\nabla P}{2\mu} z(z-h), \tag{1}$$

where z is the transverse coordinate measured from the bottom wall, and ∇P is the *local* pressure gradient. This local pressure gradient is not always equal in magnitude or direction to the overall pressure gradient, which can be denoted by $\overline{\nabla P}$. When integrated over the thickness of the fracture, from $z=0$ to $z=h$, this profile yields a local version of the cubic law,

$$\vec{Q} = -\int_0^h \vec{u}(z)dz = -h^3 \nabla P / 12\mu \,, \tag{2}$$

in which the pressure gradient is allowed to vary from point to point in the plane of the fracture.

The steady-state pressure field $P(x,y)$ is found by solving the two-dimensional Laplace equation in the region of the $x-y$ plane exterior to the obstacles, i.e.,

$$\nabla^2 P(x,y) = 0. \tag{3}$$

This condition (3) follows from applying the law of conservation of mass to eqn. (2), in the form $div\ \vec{Q}=0$. Since there can be no flow into or out of the obstacles, the pressure field must satisfy $\partial P/\partial n = 0$ along the obstacle boundaries, where n is measured along the outward unit normal vector. The external boundaries of the flow field are typically either no-flow or constant-pressure boundaries (Fig. 2).

While the obstacles are correctly treated as being impermeable in the Hele-Shaw approximation, it is not possible to impose the no-slip boundary condition along these surfaces. A well-posed boundary-value problem for Laplace's equation that leads to a unique solution requires only one boundary condition at each point of the boundary (Bers et al., 1964). The condition $\partial P/\partial n = 0$ seems seems to be mandatory, since it

reflects the fact that fluid cannot enter or leave the obstructions. Violating this condition would destroy the essential geometric features of the flow field. If we also attempted to impose a condition corresponding to the fact that the tangential velocity must vanish along the boundary, this would create an overdetermined system which would in general have no solution. Hence we must forego this additional condition, which would be written as $\partial P/\partial t = 0$, where t is the direction tangential to the obstacle boundary, even though it is physically correct. The full Navier-Stokes equations, on the other hand, do allow imposition of both the no-flow and two no-slip boundary conditions (in the two tangential directions along each solid boundary surface). Since the Navier-Stokes equations consist of three coupled second-order equations for the three velocity components, they are in effect sixth-order, and require the specification of more boundary conditions. A similar inability to satisfy the no-slip condition arises when averaging the Navier-Stokes equations over a representative elementary volume (REV), yielding a Laplace equation for the macroscopic pressure, which is then interpreted as an average pressure over the REV (Bear, 1988). Although our analysis leads to the same mathematical equation, $\nabla^2 P = 0$, in the present case P represents the local value of the pressure, and no averaging process is implied.

Since the solutions to the Hele-Shaw equations do not satisfy the no-slip boundary conditions on the sides of the obstacles, they will only be approximations to the (physically exact) Navier-Stokes solutions. Based on his method of reducing the Navier-Stokes equations to the Hele-Shaw equations, Stokes conjectured (see Lee and Fung, 1969) that the relative error of the Hele-Shaw approximations would be on the order of h/a. This assertion has been verified by Lee and Fung (1969) for the problem of flow between two parallel plates that are propped open by a single cylindrical post of radius a. They used the full Navier-Stokes equations, and computed a second-order correction to the Hele-Shaw solution. Their second-order correction to the relationship between flowrate and pressure drop was in fact proportional to h/a, as

Stokes had conjectured. Errors of this magnitude should be negligible for many applications to real fractures. For example, typical average apertures of fractures in crystalline rock are on the order of $10-100\ \mu m$, while asperity sizes (in the fracture plane) are usually on the order of millimeters (Pyrak-Nolte et al., 1987). The other assumption of the Hele-Shaw model, that of a small reduced Reynolds number, will also be satisfied in many cases of interest. For example, if we consider water with $\mu = 0.001$ Pa·s flowing in a fracture with $h = 100\,\mu m$ and $a = 10\,mm$, then the criterion $Re^* < 0.1$ implies that the pressure gradient should not exceed 10^5 Pa/m, or about 1 bar/m (5 psi/ft). While naturally occurring pressure gradients are usually not this large, this criterion could be violated in situations of forced flow, such as hydraulic fracturing processes.

METHODS OF ANALYSIS

Various methods can be used to find solutions to the Laplace equation in two dimensions, among which are many numerical, analytical and analogue techniques. We use a boundary element method as a general tool to study flow around asperities, and to find the effective fracture conductivity. Analogue measurements are used to validate the code for simple geometries, such as circular asperities. Finally, analytical methods are used to develop expressions for the effective conductivity of a fracture with randomly distributed asperities of elliptical planform.

Boundary-element analysis

The boundary-value problem described above can be solved for general obstacle shapes using any of the numerical schemes that have been constructed to treat Laplace's equation. We use a boundary-element method to solve Laplace's equation in square regions containing contact areas of various shapes (Fig. 2). Fixed pressures are maintained on two opposing edges of the region, while the other two sides are

taken to be no-flow boundaries. The boundary-element method has certain advantages over finite-differences or finite-elements for this type of problem, since it requires discretization only of the boundaries of the problem, instead of the entire flow region. Briefly described, the boundary-element method utilizes ''point-source'' type solutions to the partial differential equation, and superimposes them to satisfy the boundary conditions in some average or approximate sense. Details of the method, and some computer programs, can be found in Brebbia (1978). The code used here, FLOW, is described in detail by Chen (1990). The boundary-element calculations yield the pressure distribution throughout the flow region. The local flowrate can be found from eqn. (2), after which the total flux through the region is found by integrating the normal component of the flowrate vector across one of the constant-pressure boundaries. In the calculations, it is convenient to normalize the problem by setting $h = 1$ and $\mu = 1$, in which case the effective permeability k^* is found by dividing the flowrate magnitude $|\vec{Q}|$ by the overall pressure gradient $\overline{\nabla P}$.

Analogue measurements

Since the fluid flow is assumed to be described by Laplace's equation, with the contact areas serving as impermeable boundaries, this problem is analogous to the flow of electrical current in a thin sheet with holes punched in it (cf., Bear, 1988; Tobochnik et al., 1989). Since the holes obstruct the flow of electrical current, they are analogous to the asperity obstacles. Experiments were therefore carried out on such sheets to measure the overall electrical conductivity (which is the analogue of the fracture permeability), in order to validate the numerical code. For these experiments, a thin sheet of conductive paper is cut into a square, and a strip of metallic paint is applied to two opposing edges. Since the conductivity of the paint is much higher than that of the paper, these edges will be lines of constant potential. Holes which have the desired shapes, sizes and locations are cut out of the sheet, and the overall conductance is measured with an ohm-meter. Since resistance measurements can be

made very accurately, this method is limited only by the precision with which the holes can be cut. We used a razor-knife to cut the holes, after outlining the shapes with a pencil. This method is very precise for circular holes, or other holes with simple, smooth shapes. Precision was difficult to maintain when cutting shapes such as thin ellipses, for example.

Effective-medium theory

The problem outlined above is a typical one in the field of effective properties of heterogeneous media. The unobstructed areas between the obstacles are regions with some known permeability, k_o, while the obstacles are regions of zero permeability. The aim of an effective medium theory is to determine an effective macroscopic permeability k^* that can be used, in conjunction with Darcy's law, to model flow through the fracture on length scales large enough to encompass many asperities. Since this problem is governed by Laplace's equation, the method introduced by Maxwell to predict the electrical conductivity of a three-dimensional conductor permeated with infinitely-conductive spheres (see Carslaw and Jaeger, 1959, p. 425) can be used. This method was used by Zimmerman (1989) to model the thermal conductivity of fluid-saturated rocks, assuming the pores to be oblate spheroids, and produced reasonably accurate results. In the terminology of the present problem, Maxwell's method consists of calculating the decrease in flow due to a single obstacle of known size and shape, averaging this effect over all shapes and orientations of the obstacles, and then equating the resulting decrease in flow to that which would be caused by a single circular "obstruction" which has some effective permeability k^*. Walsh (1981) applied this method to a fracture with "randomly" located circular obstructions; here we extend this method to cases where the obstacles are elliptical in shape, with random orientations.

RESULTS

Circular obstructions

In general, the effective fracture permeability will depend on both the shape of the obstructions, and their location and orientation. The simplest case to consider is that of circular obstructions, for which the issue of orientation is not relevant. Walsh (1981) used Maxwell's effective medium approach, along with the solutions for the potential fields surrounding circular inclusions (Carslaw and Jaeger 1959, p. 426), to derive the following expression for the effective permeability of such a system:

$$\frac{k^*}{k_o} = \frac{1-c}{1+c}\,, \tag{4}$$

where c is the fractional contact area of the fracture. Walsh interpreted this result as applying to "randomly located" obstructions. However, the Maxwell formalism cannot account for correlations in the locations of the asperities. Furthermore, any deviation from randomness would introduce a higher-order effect that will not be important at the low values of c found in naturally occurring fractures, which are usually less than 0.25 (Tsang and Witherspoon, 1981). For example, the numerical calculations of Tzadka and Schulgasser (1983) for the related problem of the transverse thermal conductivity of a material containing highly-conducting cylindrical fibers show that correlations between the locations of the inclusions do not become important until c reaches about 0.50. Hence, for $0 < c < 0.25$, Walsh's result should apply equally well to random or ordered arrays of obstacles, as long as the ordered arrays lead to isotropic permeability tensors.

Boundary-element calculations were carried out for fractures with circular obstructions arranged in square arrays (see Fig. 3), for values of c ranging from 0 to 0.25. When the obstructions are arranged in a periodic array, the calculations need

only be carried out in a "unit cell" formed by the imaginary grid of intersecting no-flow and constant pressure lines. A fracture in which the circular obstructions are arranged in a square (or an hexagonal) grid will exhibit an *isotropic* two-dimensional permeability tensor (Nye, 1985, p. 23), despite the fact that the details of the velocity field will vary with direction. This seeming discrepancy is related to the fact that the velocity field is a local property, whereas the permeability is an integrated property. Hence a single calculation of the effective permeability in any convenient direction will in fact yield the permeability in all directions. With these facts in mind, we note that (see Fig. 3) the boundary-element calculations for the square array agreed very closely with the predictions of the Maxwell-Walsh expression. As an additional check on the accuracy of the boundary-element calculations, analogue electrical conductivity measurements were also carried out. The measured conductivities (see Fig. 3) were in close agreement with both the Maxwell-Walsh predictions and the boundary-element calculations.

Elliptical obstructions

Since the Maxwell effective medium theory works very well for circular obstructions, it seems reasonable to extend it to more general shapes. One shape that is often used in modeling various physical properties of rocks is the ellipse (cf., Seeburger and Nur, 1984), which has been used to model the shapes of both pores and grains in sedimentary rocks. In our problem we use the ellipse to model the planform of the fracture asperities. Although it might be thought that the ellipse, as well as the circle, are both too idealized to represent real asperities, the ellipse has the advantage that by varying the aspect ratio, one can achieve different values of the perimeter-to-area ratio.

The basic problem that must be solved in order to apply this approach to elliptical obstructions is Laplace's equation in the region exterior to an ellipse, with a uniform potential gradient at infinity, and no flow across the boundary of the ellipse. Since the

ellipse has an arbitrary angular orientation with respect to the imposed potential gradient, the effect on the flow must be averaged over all (equally likely) orientations. The perturbation in the flow field far from the obstacle is then equated to the perturbation that would be caused by an equivalent circular obstacle with some finite conductivity k^*, which leads to an equation for k^* in terms of the number density and aspect ratio of the obstacles. This basic boundary-value problem is a special case of the more general problem solved by Obdam and Veling (1987), in which the elliptical obstacle has a finite conductivity. The details of the utilization of their solution for the computation of the effective permeability of a fracture containing a random distribution of elliptical asperities are described in Appendix A. The resulting expression for the effective permeability is similar in form to eqn. (4) for circular obstructions, but with the percentage contact area c multiplied by a factor that depends on the shape of the ellipse:

$$\frac{k^*}{k_o} = \frac{1-\beta c}{1+\beta c}, \qquad \text{where} \quad \beta = \frac{(1+\alpha)^2}{4\alpha}, \tag{5}$$

and the aspect ratio of the ellipse, α, is defined as the ratio of the minor to major axis. For circular obstructions, $\alpha = 1$, and $\beta = 1$, and so expression (5) reduces to Walsh's expression, eqn. (4).

The factor β defined in eqn. (5) is always greater than unity, and monotonically increases as the ellipse becomes more elongated. Since $(1-\beta c)/(1+\beta c)$ is less than $(1-c)/(1+c)$ for all $0<c<1$ when $\beta>1$, as can be shown by cross-multiplying and expanding out the terms, the k^*/k_o curves for elliptical obstructions will always lie below Walsh's curve. This is consistent with the fact that Walsh's expression coincides with the upper bound on k^*/k_o that was derived by McCoy (1982) using variational principles. The predictions of the effective medium theory for $\alpha=0.2$ are shown

in Fig. 4, where they are compared to boundary-element calculations. The elliptical obstacles were generated by centering them on alternate squares in a square array (such as the black squares on a checkerboard) and then assigning to each ellipse a randomly chosen angular orientation (see Fig. 4). Grids encompassing varying number of square cells were used, and it was found that grids of 30×30 cells were sufficient to eliminate the significance of edge effects. Over the range of contact areas shown in the figure, $0 < c < 0.05$, the estimates of the effective medium theory are very accurate. Higher contact areas could have been achieved by placing asperities in each cell, rather than in every other cell. With ellipses of aspect ratio 0.2, the obstacles would begin to overlap each other when c reached about 0.15. However, since higher contact area concentrations require a much larger number of computational nodes, we did not use values of c greater than 0.05.

Due to the laborious and painstaking procedure required to cut out the elliptical holes in the conductive sheet, only one analogue measurement was made for the elliptical case. The one conductivity value measured was in fairly close agreement (see Fig. 4) with the predictions of eqn. (5).

Irregular obstructions

The shapes of asperity obstructions found in real rock fractures are of course more irregular than circles or ellipses. We have therefore also used our boundary-element code to study flow around irregularly shaped obstacles such as those shown in the inset of Fig. 5. These patterns are generated by breaking up a square flow region into a 30×30 rectangular grid, and assigning each grid block to be either an obstruction zone or a flow zone. This assignment process, which is described in detail by Coakley (1989) and Chen (1990), is discussed briefly in Appendix B. Examples of such simulations, using the value 0.75 for the correlation parameter λ (defined in Appendix B), are shown in Fig. 5. The computed permeabilities all lie below Walsh's curve, as indeed they must, since eqn. (4) is an upper bound with respect to all

possible obstruction geometries that generate isotropic permeability tensors.

In order to draw general conclusions from results such as those shown in Fig. 5, it would be useful to have some way to quantify the obstruction geometry. One possibility, which would make use of the previously-discussed analytical expressions for a fracture with elliptical obstructions, would be to assign to each fracture geometry a suitably chosen ''equivalent aspect ratio''. In analogy with the Carman-Kozeny equation (Scheidegger, 1974) for the permeability of three-dimensional porous media, for example, an aspect ratio could be chosen based on the total area and total perimeter of the actual asperities. As a test of this conjecture, consider the geometry shown in the inset of Fig. 5. Using a length scale in which each small square is of unit length, this geometry has 21 obstacles with average area of 8.57, and average perimeter of 14.0. If we ''replace'' these obstacles by 21 ellipses, each of area 8.57, the aspect ratio would have to be 0.258 in order to maintain the same average obstacle perimeter. With this value of α used for all values of c in the suite of data shown in Fig. 5, the normalized permeabilities predicted by eqn. (5) are shown by the solid line. The agreement between these predictions and the numerically computed values is fairly good, suggesting that the conductivity of a fracture with an irregular contact-area geometry can be modeled by eqn. (5), with the aspect ratio chosen so as to give the correct values for the average perimeter and average area of the individual obstacles. Use of this rule-of-thumb for other asperity geometries generated by the algorithm described in Appendix B (see Chen, 1990 for additional examples) leads to the same reasonably close agreement between computed and predicted permeabilities as shown in Fig. 5.

CONCLUSIONS

Numerical, analogue and analytical methods have been used to investigate the effect of contact area geometry on the permeability of a fracture. To isolate the effect

of contact area, the fracture aperture has been assumed constant in the regions between the asperities. For obstacles that are circular in the plane of the fracture, eqn. (4) derived by Walsh (1981) using the Maxwell effective medium approximation was found to be very accurate for contact areas up to at least 25%. The Maxwell-Walsh approach was extended to randomly oriented obstacles of elliptical shape (eqn. (5)), with the results verified numerically for $\alpha = 0.2$, $c \leq 0.05$. Fractures with more irregular contact area geometries were also studied using the boundary-element method. Such fractures had permeabilities that were lower, by as much as 30%, than would be predicted by Walsh's expression, but which could be fit fairly well by the effective medium approximation if an equivalent aspect ratio is used. This equivalent aspect ratio can be chosen by imagining the actual asperities to be replaced by an equal number of ellipses with the same total area and the same total perimeter.

ACKNOWLEDGEMENTS

This work was supported by the Director, Office of Civilian Radioactive Waste Management, Repository Technology and Transportation Division, and by the Director, Office of Energy Research, Office of Basic Energy Sciences, under U.S. Department of Energy Contract DE-AC03-76SF00098. The authors thank Larry Myer and Peter Persoff of LBL for reviewing this paper.

APPENDIX A

In this appendix, we present the derivation of eqn. (5) for the effective permeability of a fracture that is partially obstructed by randomly-oriented and randomly-located elliptical asperities. We use the method originally devised by Maxwell to find the effective conductivity of a three-dimensional body containing a dispersion of infinitely-conductive spheres. Since this method entails the calculation of the perturbative effect that a single obstruction has on the flow field, but does not consider the interactive effects of pairs (or triples, etc.) of obstructions, it is generally considered to be rigorously correct only to first order in the inclusion concentration. However, evidence from further analysis of the three-dimensional spherical inclusion problem (Zuzovsky and Brenner, 1977) implies that this method is actually correct up to at least second order, with a range of accuracy extending to inclusion concentrations of at least 0.25.

Consider now an elliptical obstacle, with semi-major and semi-minor axes a and αa, placed in a uniform flow field, with the direction of the free-stream velocity vector (of magnitude Q_o) oriented at an angle δ to the major axis of the ellipse (Fig. A1). Let the coordinate axes of a complex plane $z = x + iy$ be centered on the ellipse, and aligned so that the free-stream velocity is in the x direction. (This complex variable z should not be confused with the Cartesian coordinate z that is perpendicular to the $x-y$ plane, as in Fig. 1). Obdam and Veling (1987) found the complex velocity potential in the general case where there is an arbitrary ratio of the permeability inside the obstacle to the permeability outside of the obstacle. The solution to our problem is found by setting this ratio equal to zero, in which case the complex velocity potential exterior to the ellipse is given by

$$\Omega(z) = -Q_o \left[\zeta e^{-i\delta} + \frac{a^2(1+\alpha)(\alpha\cos\delta + i\sin\delta)}{\zeta + \sqrt{\zeta^2 - a^2(1-\alpha^2)}} \right], \qquad \text{(A1)}$$

where $\zeta = ze^{i\delta}$. Note that Obdam and Veling (1987) aligned their coordinate axes with the ellipse; since we want to consider a distribution of ellipses randomly oriented with respect to a fixed macroscopic flow field, we find it convenient to align the axes with the free-stream velocity vector. This requires rotating their coordinate system by an angle δ, *i.e.*, letting $z \rightarrow ze^{i\delta}$.

At distances far from the ellipse, the denominator in the term on the right side of eqn. (A1) reduces to 2ζ, and the velocity potential takes the form

$$\Omega(z) \approx -Q_o\left[z + \frac{a^2(1+\alpha)(\alpha\cos\delta + i\sin\delta)}{2ze^{i\delta}}\right]. \tag{A2}$$

The complex velocity vector $Q_x + iQ_y$ is related to the potential Ω by $Q_x - iQ_y = -\Omega'(z)$, so that we find, for large $|z|$,

$$Q_x + iQ_y \approx Q_o\left[1 - \frac{a^2(1+\alpha)(\alpha\cos\delta - i\sin\delta)e^{i\delta}}{2\bar{z}^2}\right], \tag{A3}$$

where $\bar{z}$ denotes the complex conjugate $x - iy$. Using the polar representation for z on the right side, we have $z = re^{i\theta}$, and $\bar{z}^2 = r^2e^{-i2\theta}$, so

$$Q_x + iQ_y \approx Q_o\left[1 - \frac{a^2(1+\alpha)(\alpha\cos\delta - i\sin\delta)e^{i\delta}e^{i2\theta}}{2r^2}\right]. \tag{A4}$$

Now imagine that there are N ellipses, each with the same aspect ratio α, but with a random distribution of orientation angles δ. Neglecting the (higher-order) effect of flow-field perturbations due to pairs, triples, etc., of nearby obstacles, the total velocity

field far from the obstacles is given by

$$Q_x + iQ_y \approx Q_o\left[1 - \frac{Na^2(1+\alpha)<(\alpha\cos\delta - i\sin\delta)e^{i\delta}>e^{i2\theta}}{2r^2}\right], \tag{A5}$$

where the brackets denote an average taken over all possible orientations, from $\delta=-\pi/2$ to $\delta=+\pi/2$. Note that θ is measured with respect to the fixed coordinate system, and does not vary with the orientation of the elliptical obstacle. The bracketed average in eqn. (A5) can be evaluated as follows:

$$<(\alpha\cos\delta - i\sin\delta)e^{i\delta}> = <(\alpha\cos\delta - i\sin\delta)(\cos\delta + i\sin\delta)>$$

$$= <(\alpha\cos^2\delta + \sin^2\delta) - i(1-\alpha)(\sin\delta\cos\delta)>$$

$$= \frac{1}{\pi}\int_{-\pi/2}^{\pi/2}(\alpha\cos^2\delta + \sin^2\delta)d\delta - i(1-\alpha)\frac{1}{\pi}\int_{\pi/2}^{\pi/2}(\sin\delta\cos\delta)d\delta$$

$$= \frac{1+\alpha}{2}. \tag{A6}$$

The far-field velocity vector is therefore given by

$$Q_x + iQ_y \approx Q_o\left[1 - \frac{Na^2(1+\alpha)^2}{4r^2}e^{i2\theta}\right]. \tag{A7}$$

The solution of Obdam and Veling (1987) can also be used to find the velocity field that would exist around a circular obstacle of radius A and permeability k^* that perturbs a uniform flow field in a medium with permeability k_o. This solution is found by putting $\alpha = 1$ and $k^{in}/k^{out} = k^*/k_o$ in their general solution, yielding

$$Q_x + iQ_y = Q_o \left[1 - \frac{(k_o - k^*)A^2}{(k_o + k^*)r^2} e^{i2\theta} \right] . \tag{A8}$$

If the ensemble of N obstacles can be replaced by an equivalent homogeneous region with permeability k^*, then the two velocity fields given by eqns. (A7) and (A8) must be equal, implying that

$$\frac{k_o - k^*}{k_o + k^*} = \frac{(1+\alpha)^2}{4\alpha} c \ , \tag{A9}$$

where $c = N\pi a^2 \alpha / \pi A^2$ is the area fraction of the elliptical obstacles. When solved for the ratio k^*/k_o, eqn. (A9) yields eqn. (5).

As partial checks on the correctness of these calculations, first note that for circular inclusions, $\alpha = 1$, and eqn. (A9) reduces to Walsh's expression, eqn. (4). In the other limiting case of small aspect ratio, eqn. (A9) agrees to first order in c with the first-order calculations of Tobochnik et al. (1989), who found $k^*/k_o = 1 - c/2\alpha$.

APPENDIX B

In this appendix we describe briefly the procedure used to generate irregular obstacle patterns, such as shown in the insert of Fig. 5. A more detailed discussion of this procedure is given by Coakley (1989). First, we break up a square region that represents a fracture plane into a grid of, say, 30×30 squares. These squares can be labeled with the indices $\{i,j\}$, reading left to right, starting in the upper left corner, as would be done in labeling the elements of a matrix. Next, each square is assigned an independent, log-normally distributed random variable, X_{ij}. We then convolute X_{ij} with a moving-average filter, H_{kl}, to get a spatially-correlated, log-normally distributed random variable, Y_{ij}, as follows:

$$Y_{ij} = \sum_{k=-D}^{D} \sum_{l=-D}^{D} X_{(i-k)(j-l)} H_{kl} \,. \tag{B1}$$

The filter weights H_{kl} are radially-symmetric, and decay exponentially according to

$$H_{kl} = \exp(-\lambda\sqrt{k^2+l^2}) \quad \text{for} \quad \sqrt{k^2+l^2} \le D \,, \tag{B2}$$

and $H_{kl}=0$ for $\sqrt{k^2+l^2}>D$, where D is a parameter that determines the spatial size of the filter, and λ is a damping factor which determines the rate at which the filter weights decay to zero. The variable Y_{ij} can be thought of as the aperture, h, of a rough-walled fracture. Finally, we chose a clipping level Y_o, and designate all squares with $Y_{ij} \ge Y_o$ to be open void areas, which are assigned an aperture of h. All squares with $Y_{ij} < Y_o$ are designated to be closed contact regions. The clipping level Y_o can be varied until the desired contact area percentage is achieved. This algorithm was used in a larger study in which the mechanical closure of rough-walled fractures was

also modeled numerically; for these purposes the apertures would not be clipped off above $Y_{ij} = Y_o$.

This procedure generates a simulated fracture plane that contains irregularly-shaped islands of asperity contact. If we had not convoluted the variables X_{ij} with the filter weights H_{kl}, the clipping procedure would have led, in general, to a very large number of small contact areas, many of which were only one square in size. The convolution process introduces spatial correlation into the random aperture field. In our simulations, the filter radius D was always chosen to be 7.5, while the damping factor λ was varied from 0.25 to 3.0. Since the exponentially-decreasing filter weights H_{kl} decay to 0 as k and l increase, the use of a finite cutoff value D in eqn. (B2) is merely a numerical convenience that has little effect on the results. Larger values of λ lead to contact islands that are more dispersed, whereas smaller values of λ lead to fewer but larger islands of contact. Since the permeability of a fracture modeled by the Hele-Shaw equations (which are valid as long as the typical diameter of an island a is much larger than the aperture h) should not depend on the size of the contact islands, but only on their planform, the value of λ turns out to have little influence on the resulting permeabilities, provided that it is not so large that all correlation dies off within a distance less than one unit square. The results presented in Fig. 5 were for the case of $\lambda = 0.75$; results for other values of λ can be found in Chen (1990).

REFERENCES

Bear, J., 1988. Dynamics of Fluids in Porous Media. Dover Publications, New York.

Bers, L., John, F., and Schechter, M., 1964. Partial Differential Equations. Wiley-Interscience, New York.

Brebbia, C.A., 1978. The Boundary Element Method for Engineers. Pentech Press, London.

Brown, S.R., 1987. Fluid flow through rock joints: the effect of surface roughness. J. Geophys. Res., B92: 1337-1347.

Carslaw, H.S., and Jaeger, J.C., 1959. Conduction of Heat in Solids. Oxford University Press, Oxford.

Chen, D.W., 1990. Coupled stiffness-permeability analysis of a single rough-surfaced fracture by the three-dimensional boundary-element method. Ph.D. thesis, University of California, Berkeley, Calif.

Chen, D.W., Zimmerman, R.W., and Cook, N.G.W., 1989. The effect of contact area on the permeability of fractures. Proc. 30th U.S. Symp. on Rock Mech., (A.W. Khair, ed.), pp. 81-88. Balkema, Rotterdam.

Coakley, K., 1989. Spatial statistics for predicting flow through a single rock fracture. Ph.D. thesis, Stanford University, Stanford, Calif.

Lee, J.S., and Fung, Y.C., 1969. Stokes flow around a circular cylindrical post confined between two parallel plates. J. Fluid Mech., 37: 657-670.

McCoy, J.J., 1982. Bounds on the transverse effective conductivity of computer-generated fiber composites. J. Appl. Mech., 49: 319-326.

Nye, J.F., 1985. Physical Properties of Crystals. Oxford University Press, Oxford.

Obdam, A.N.M., and Veling, E.J.M., 1987. Elliptical inhomogeneities in groundwater flow - an analytical description. J. Hydrol., 95: 87-96.

Pyrak-Nolte, L.J., Myer, L.R., Cook, N.G.W. and Witherspoon, P.A., 1987. Hydraulic and mechanical properties of natural fractures in low permeability rock. Proc. 6th Int. Cong. Rock Mech., (G. Herget and S. Vongpaisal, eds.), pp. 225-231. Balkema, Rotterdam.

Pyrak-Nolte, L.J., Cook, N.G.W., and Nolte, D.D., 1988. Fluid percolation through single fractures. Geophys. Res. Letts., 15: 1247-1250.

Schlichting, H., 1968. Boundary-Layer Theory, 6th Ed. McGraw-Hill, New York.

Seeburger, D.A., and Nur, A., 1984. A pore space model for rock permeability and bulk modulus. J. Geophys. Res., B89: 527-536.

Tobochnik, J., Dubson, M.A., Wilson, M.L., and Thorpe, M.F., 1989. Conductance of a plane containing random cuts. Phys. Rev. A, 40: 5370-5376.

Tsang, Y.W., and Witherspoon, P.A., 1981. Hydromechanical behavior of a deformable rock fracture subject to normal stress. J. Geophys. Res., B86: 9287-9298.

Tzadka, U., and Schulgasser, K., 1983. Effective properties of fiber-reinforced materials. J. Appl. Mech., 50: 828-834.

Walsh, J.B., 1981. The effect of pore pressure and confining pressure on fracture permeability. Int. J. Rock Mech., 18: 429-435.

Zimmerman, R.W., 1989. Thermal conductivity of fluid-saturated rocks. J. Petrol. Sci. Eng., 3: 219-227.

Zimmerman, R.W., Kumar, S., and Bodvarsson, G.S., 1991. Lubrication theory analysis of the permeability of rough-walled fractures. Int. J. Rock Mech., 28: 325-331.

Zuzovsky, M., and Brenner, H., 1977. Effective conductivities of composite materials composed of cubic arrangements of spherical particles embedded in an isotropic matrix. Zeit. Ang. Math. Phys., 28: 979-992.

FIGURE CAPTIONS

Fig. 1. Side view of a rock fracture (top); idealized fracture with parallel walls and isolated asperities (middle and bottom). The aperture is h, and the characteristic asperity dimension is a.

Fig. 2. Schematic diagram of the basic computational problem, showing two asperities, the no-flow and constant-pressure boundaries, and the discrete nodal points used in the boundary-element calculations.

Fig. 3. Normalized permeability of a fracture with circular asperities. Asperity geometry (for $c = 0.15$) is shown in the inset. Calculations and measurements were performed on a unit cell consisting of one circular obstacle centered within a square region.

Fig. 4. Normalized permeability of a fracture with elliptical asperities of aspect ratio 0.2. Asperity geometry (one quadrant; for $c = 0.05$) is shown in the inset. Calculations were carried out on a 30×30 grid, containing 450 ellipses. To illustrate the sensitivity of the effective medium theory (eqn. (5)) to the aspect ratio, curves are shown for $\alpha = 0.1$, 0.2, and 0.3.

Fig. 5. Normalized permeability of a fracture with irregular asperities, generated by the algorithm described in Appendix B. Example of asperity geometry used in simulations (for $c = 0.20$, on a 30×30 grid) is shown in the inset. Equivalent aspect ratio of 0.258 corresponds to an ellipse having the same average area and average perimeter as do the irregular asperities.

Fig. A1. Elliptical obstacle of aspect ratio α, with its major axis oriented at an angle δ to the free stream velocity of magnitude Q_o.

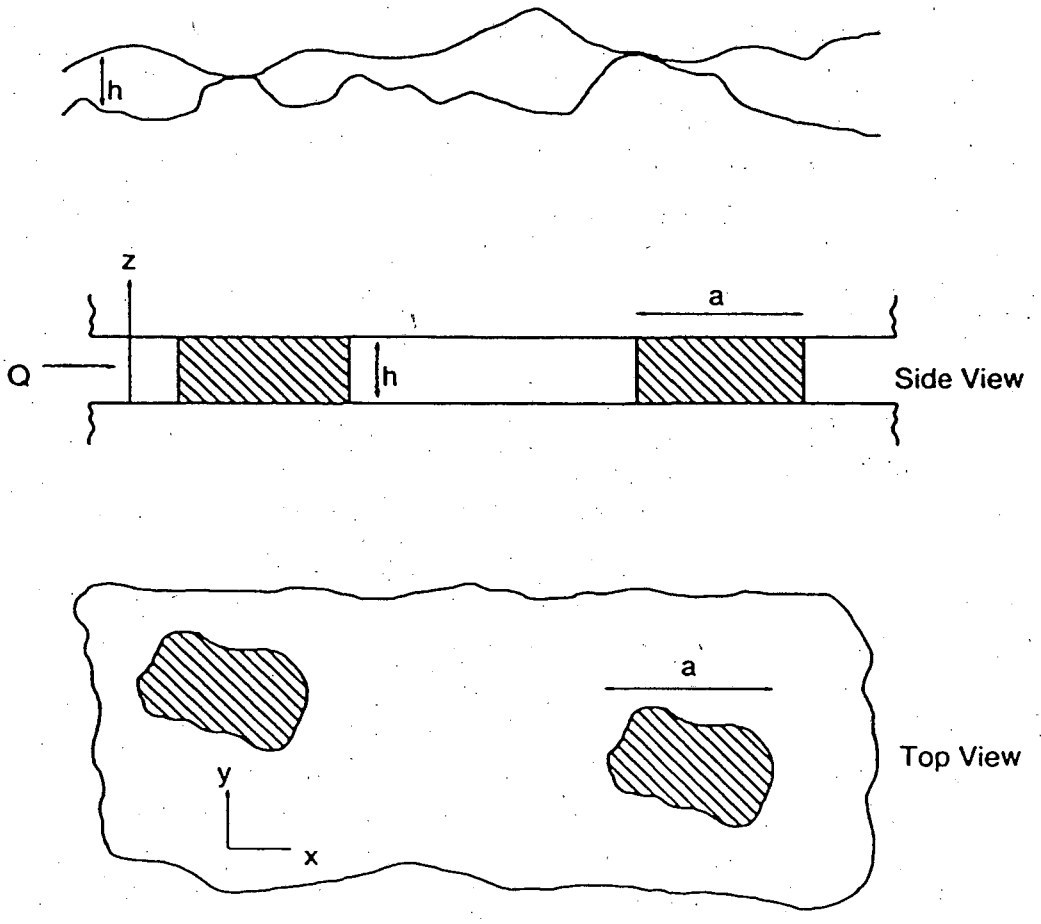

Fig. 1. Side view of a rock fracture (top); idealized fracture with parallel walls and isolated asperities (middle and bottom). The aperture is h, and the characteristic asperity dimension is a.

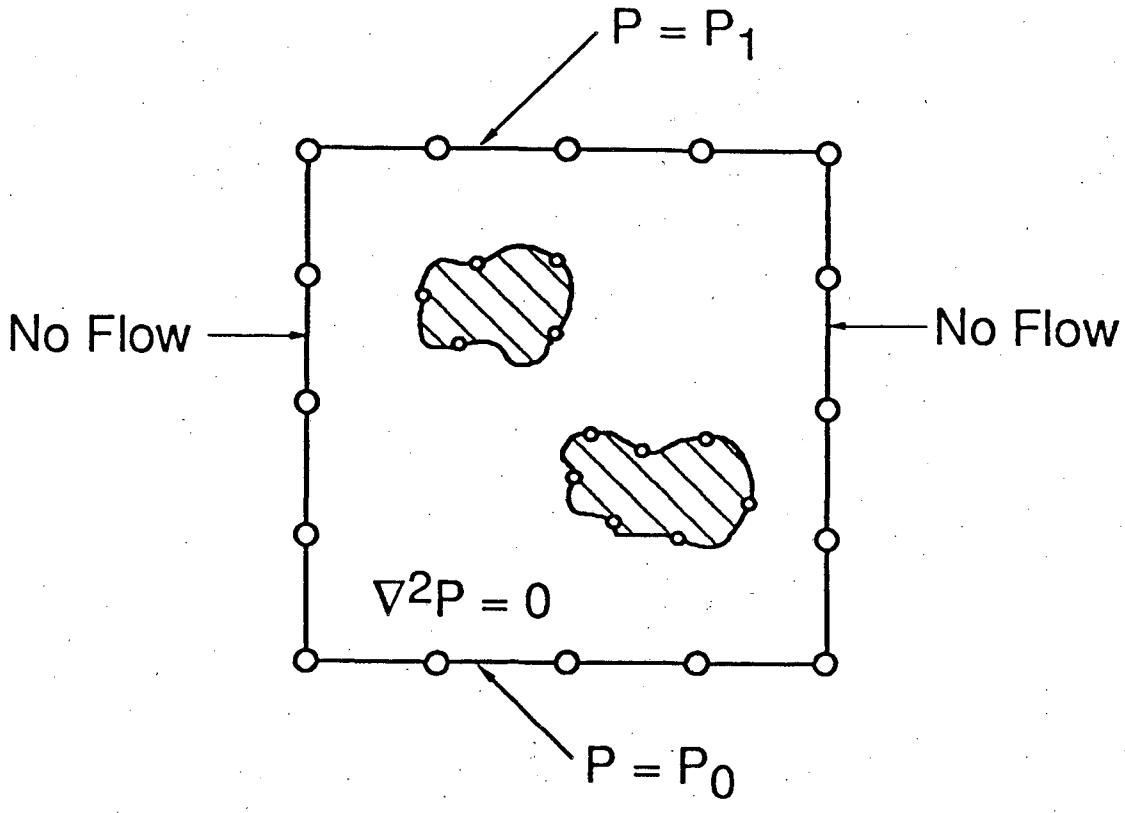

Fig. 2. Schematic diagram of the basic computational problem, showing two asperities, the no-flow and constant-pressure boundaries, and the discrete nodal points used in the boundary-element calculations.

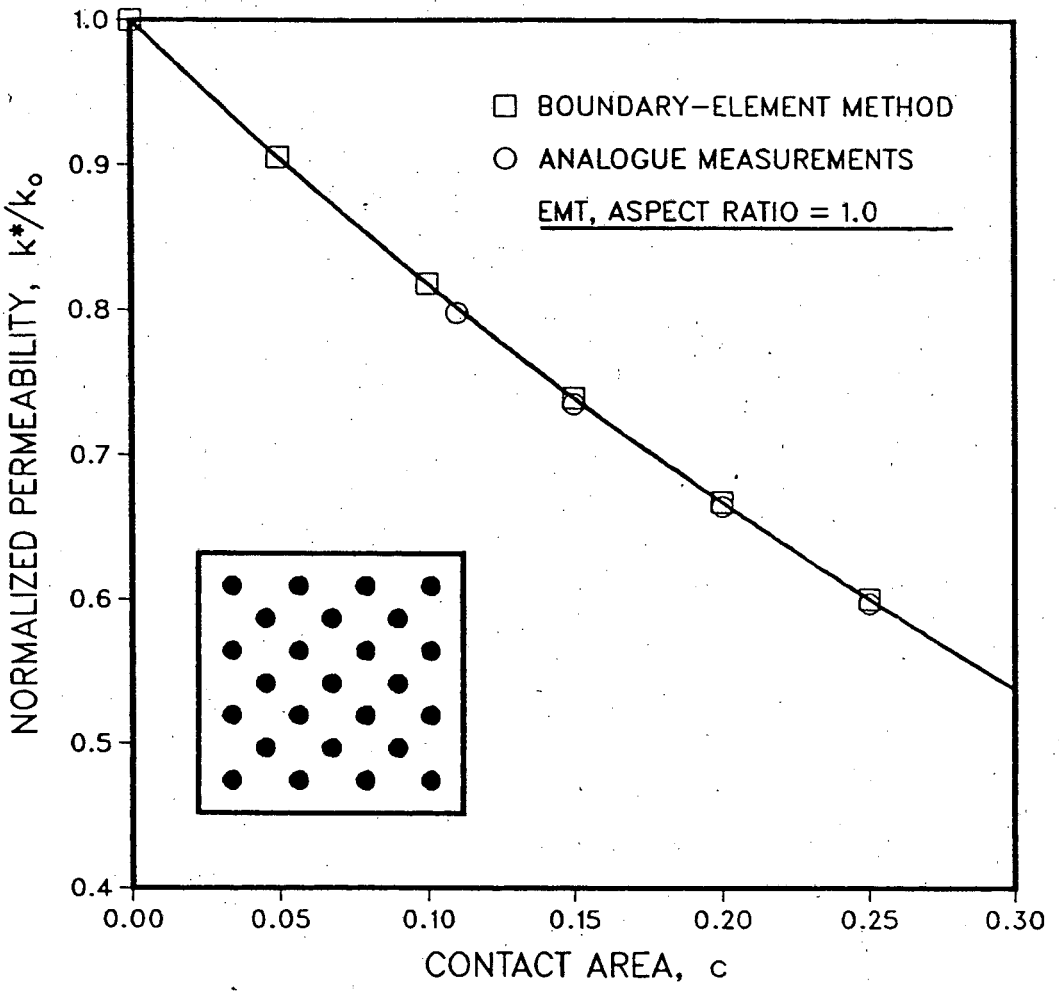

Fig. 3. Normalized permeability of a fracture with circular asperities. Asperity geometry (for $c = 0.15$) is shown in the inset. Calculations and measurements were performed on a unit cell consisting of one circular obstacle centered within a square region.

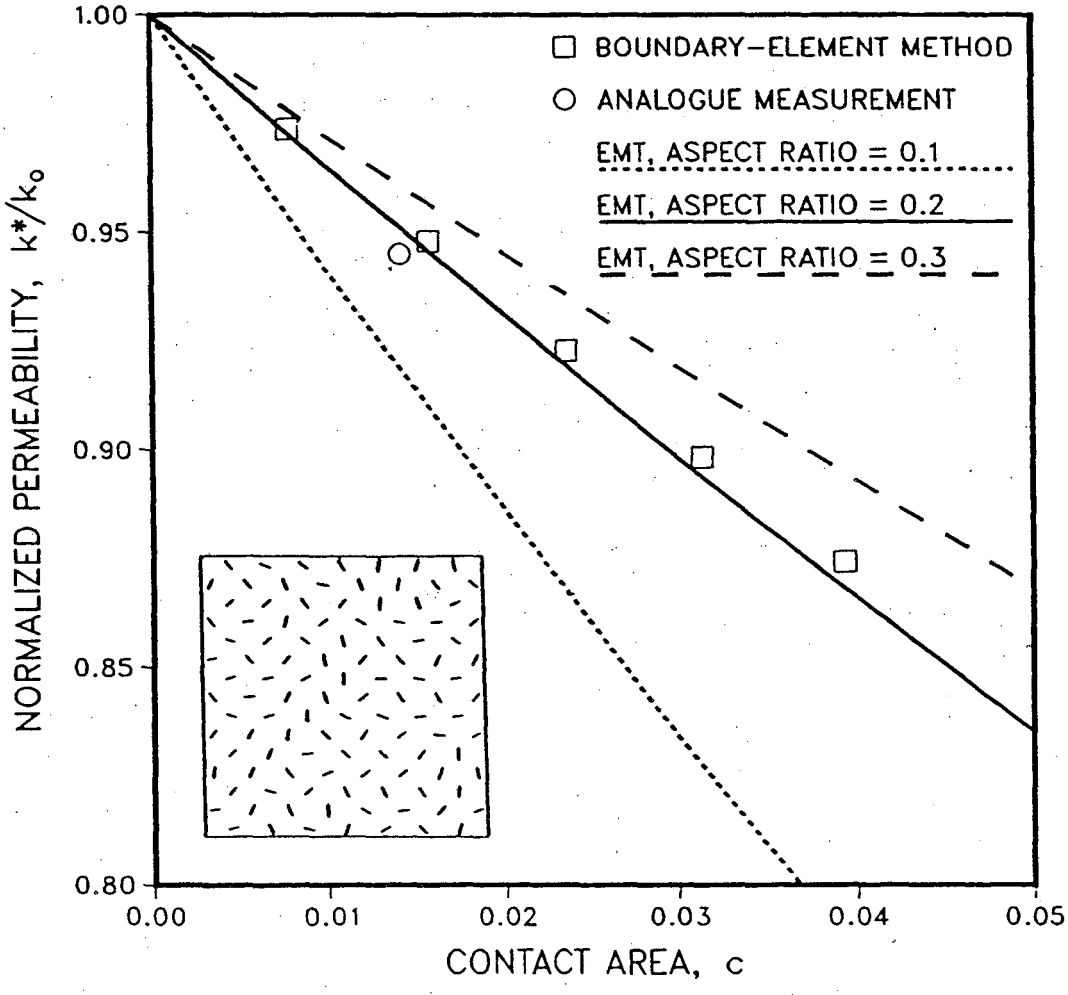

Fig. 4. Normalized permeability of a fracture with elliptical asperities of aspect ratio 0.2. Asperity geometry (one quadrant; for $c = 0.05$) is shown in the inset. Calculations were carried out on a 30×30 grid, containing 450 ellipses. To illustrate the sensitivity of the effective medium theory (eqn. (5)) to the aspect ratio, curves are shown for $\alpha = 0.1$, 0.2, and 0.3.

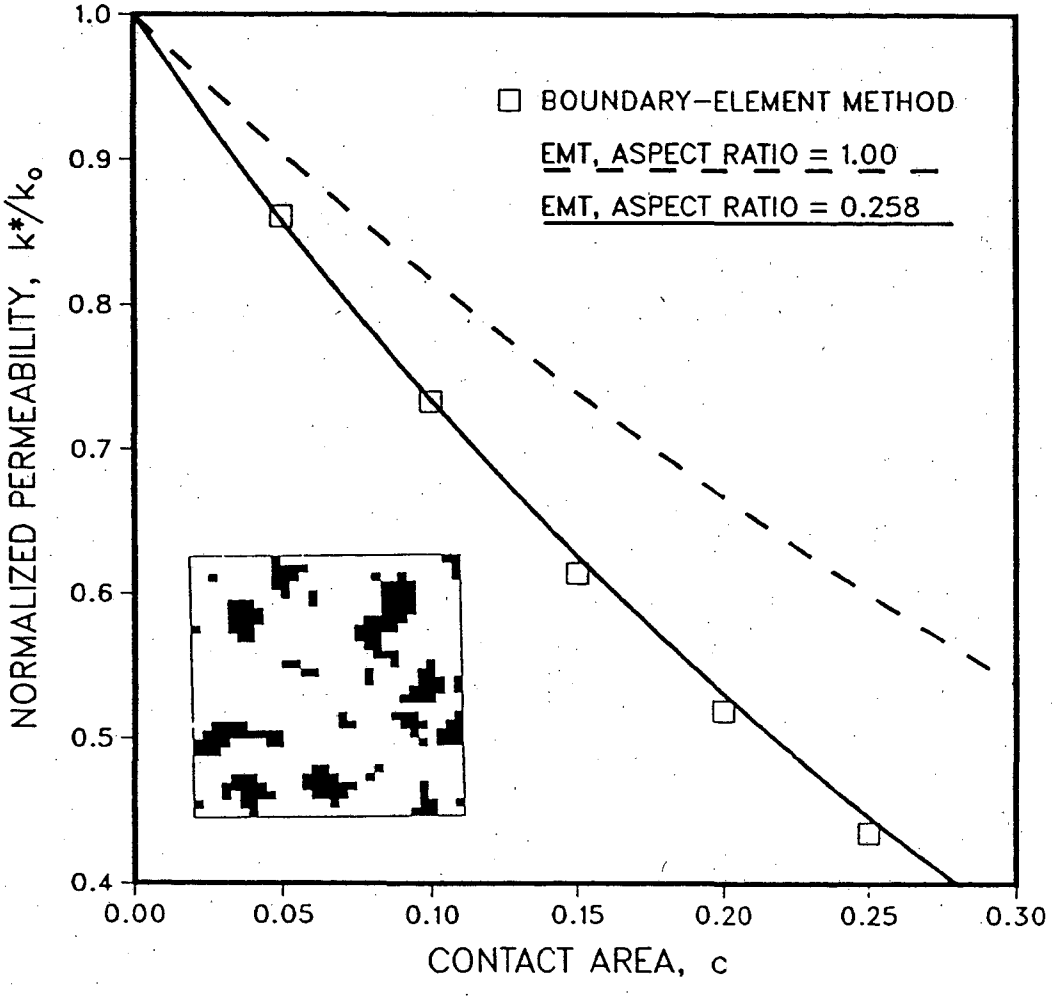

Fig. 5. Normalized permeability of a fracture with irregular asperities, generated by the algorithm described in Appendix B. Example of asperity geometry used in simulations (for $c = 0.20$, on a 30×30 grid) is shown in the inset. Equivalent aspect ratio of 0.258 corresponds to an ellipse having the same average area and average perimeter as do the irregular asperities.

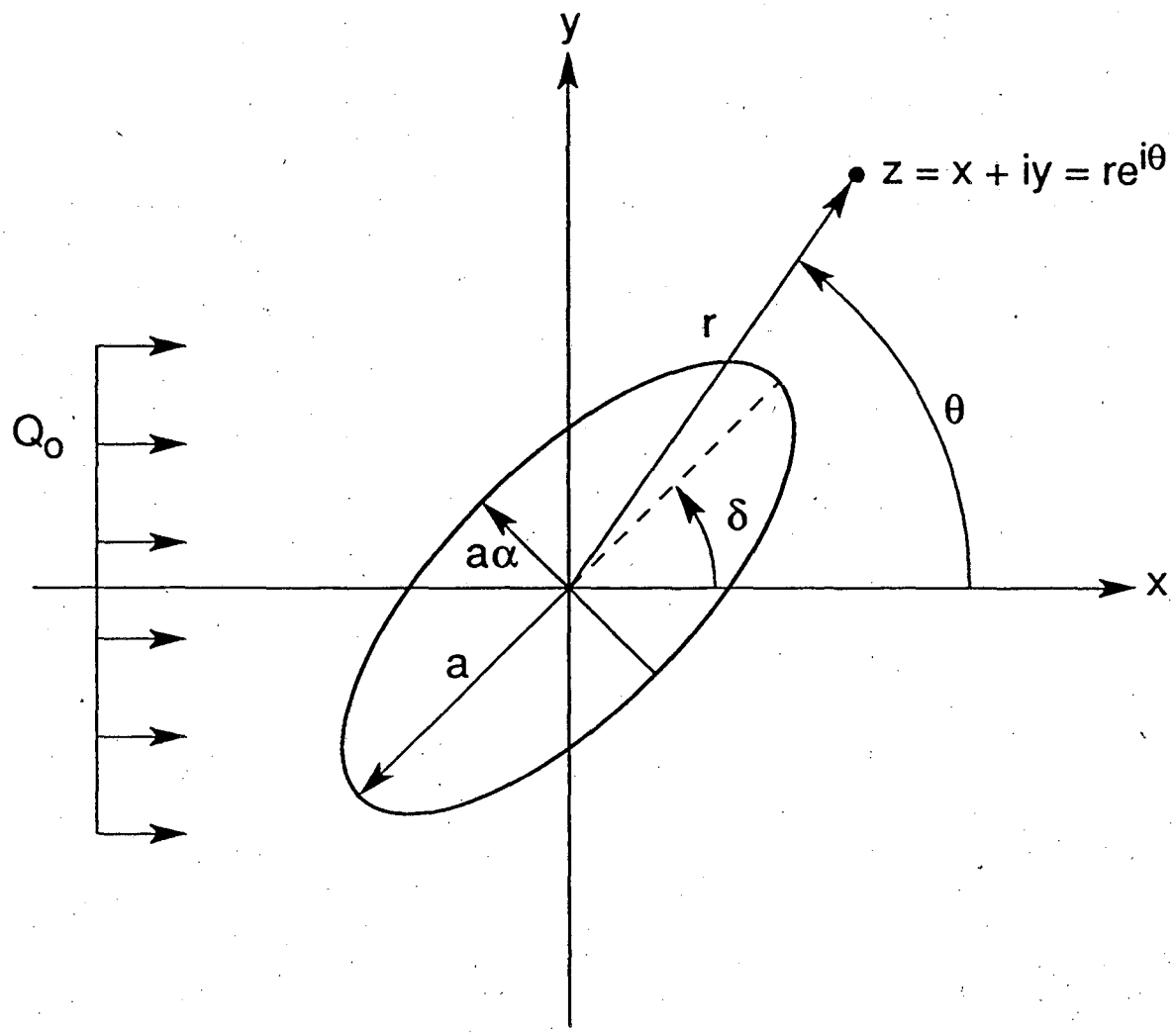

Fig. A1. Elliptical obstacle of aspect ratio α, with its major axis oriented at an angle δ to the free stream velocity of magnitude Q_o.

LAWRENCE BERKELEY LABORATORY
UNIVERSITY OF CALIFORNIA
TECHNICAL INFORMATION DEPARTMENT
BERKELEY, CALIFORNIA 94720